Macromolecules

pubs.acs.org/Macromolecules Article

Harnessing Zone Annealing to Program Directional Motion of Nanoparticles in Diblock Copolymers: Creating Periodically Well-Ordered Nanocomposites

Jiabin Gu, Runrong Zhang, Liangshun Zhang,* and Jiaping Lin*

Cite This: *Macromolecules* 2020, 53, 2111−2122 Read Online

ACCESS | Metrics & More | Article Recommendations | Supporting Information

ABSTRACT: The integration of the dynamic self-consistent field theory for polymer molecules and molecular dynamics for nanoparticles is proposed to model the structural evolution of nanocomposites in the course of zone annealing. Using computational modeling, we establish an effective approach to simultaneously tailor the spatial regularity of self-assembled nanostructures of diblock copolymers and the arrangement of nanoparticles within the matrix. As the spatially localized, mobile field of zone annealing is introduced into the hybrid organic/inorganic system, the nanocomposites re-assemble from the defective nanopatterns to the periodically well-ordered nanostructures, with the nanoparticles dispersed in the energetically favorable domains. In particular, because of the presence of response layers of diblock copolymers at the annealing front, the directional motion of nanoparticles within the matrix can be achieved by finely tuning the moving velocity and minimum Flory−Huggins interaction parameter of zone annealing. Furthermore, the regularity of self-assembled nanostructures and the spatial arrangement of nanoparticles are affected by the physiochemical properties of nanoparticles. Our theoretical findings present new opportunities to kinetically manipulate the self-assembled nanostructures of both the organic and inorganic components, which will impart their collective properties and the ultimate performances of nanocomposites.

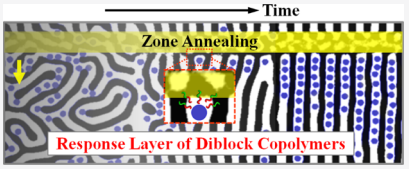

1. INTRODUCTION

Assemblies of inorganic nanoparticles (NPs) provide unique opportunities for the development of next-generation nanodevices utilizing their collective optical, electronic, and magnetic properties,[1−4] which arise from the precise organization of NPs within the structural matrix. Up to now, considerable advancements have been made in the organization of NPs into the addressable, well-ordered arrays due to a growing list of promising applications in energy harvesting and storage and microelectronic and light manipulation.[5,6] As one of the most popular strategies, templated assembly (e.g., small molecules, polymers, and DNA strands as templates or scaffolds) is a low-cost and simple route for creating the ordered assemblies of NPs.[7−11] In particular, diblock copolymers, which are composed of chemically distinct blocks linked by covalent bonds, have the capability to spontaneously assemble into a spectrum of well-defined nanostructures.[12−14] These structures on the nanometer scale can serve as the scalable scaffolds to controllably manipulate the spatial arrangement of NPs within the polymeric matrix.[15−17] However, the conventional self-assembly of diblock copolymer/NP mixtures cannot completely realize the well-ordered nanostructures due to the inherent propensity of kinetic arrest in meta-stable states for the hybrid organic/inorganic system.

For the system of pure diblock copolymers, experimentalists have prescribed a diversity of strategies to yield the well-ordered nanopatterns over the macroscopic length scale, such as the utilization of chemical or topographical templates,[18,19] shear flow,[20] and electric[21] and thermal fields.[22,23] Among the strategies mentioned above, zone annealing exerts the spatially and temporally thermal gradient fields to the samples of diblock copolymer films.[24,25] Specifically, the structural evolution of nanopatterns with lots of defects is restricted to a narrow region of annealed zones followed by their movement throughout the entire samples. In comparison with the conventional oven annealing for diblock copolymer films, zone annealing has been proven to be a versatile and efficient route for reconstructing the nanostructures with a lower defect density by overcoming the energy barriers of arrested defects within a short period.[26−28] Therefore, it is highly desirable to propose a cooperative strategy that utilizes the templated assembly of NPs together with the zone annealing of diblock copolymers,[29,30] to create the hybrid materials satisfying application-determined requirements (i.e., well-ordered nanostructures of nanocomposites and well-defined assemblies of NPs). However, the study of the self-assembly kinetics of such a hybrid system subject to the zone annealing is still lacking. There remains an urgent demand for great progress in terms of the essential mechanism of self-assembly and the evolution of

Received: January 15, 2020
Revised: February 26, 2020
Published: March 11, 2020

Downloaded via EAST CHINA UNIV SCIENCE & TECHLGY on October 23, 2020 at 11:39:35 (UTC).
See https://pubs.acs.org/sharingguidelines for options on how to legitimately share published articles.

ACS Publications © 2020 American Chemical Society

https://dx.doi.org/10.1021/acs.macromol.0c00101
Macromolecules 2020, 53, 2111−2122

self-assembled structures, which will help the experimentalists to rationally construct multifunctional nanodevices.

Computer modeling and simulations on the mesoscopic scale are playing an ever-growing and far-reaching role in the exploration of the complicated self-assembly of diblock copolymer/NP mixtures.[31−39] In our previous study, the hybrid particle-field model originally proposed by Fredrickson's group[40] (i.e., the integration of the static self-consistent field theory for diblock copolymers with Brownian dynamics for NPs) was extended to predict the hierarchically self-assembled structures of nanocomposites.[41,42] One limitation of this model is a lack of structural evolution for the hybrid organic/inorganic system. Recently, on the basis of the dynamic self-consistent field theory (DSCFT),[43,44] we developed a zone-annealing model to examine the self-assembly kinetics of pure diblock copolymers.[45−47] It is successfully demonstrated that the defect-free structures of diblock copolymers can be achieved by the mechanism of defect annihilation after the incorporation of zone annealing, which is in line with the experimental observations. The success of DSCFT makes it ready to be extended to predict the self-assembly behaviors of diblock copolymer/NP mixtures.

In the present work, a novel method that integrates DSCFT for diblock copolymers with the molecular dynamics (MD) for NPs is developed to probe the self-assembly behaviors of zone-annealed nanocomposites. Such an integrated method is applied to investigate the effects of zone annealing and NPs' incorporation on the ordering degree of self-assembled nanostructures and the spatial arrangement of NPs. Beyond obtaining the equilibrium structures, the sophisticated method can capture the structural evolution and ordering mechanism of diblock copolymer/NP mixtures, which cannot be resolved by the experimental observations and equilibrium simulations. Furthermore, the experimental realization of well-ordered nanostructures is discussed, where we point out the wide implication of these results for rationally designing the multifunctional nanodevices.

2. COMPUTATIONAL MODELING AND METHOD

We couple DSCFT with MDs to probe the ordering behaviors of zone-annealed nanocomposites, which contain a mixture of n_c AB diblock copolymers and n_P spherical NPs (designated as P). The AB diblock copolymers are specified by the Gaussian chains with ideal gyration radius R_g and length N. The volume fraction of A blocks in the polymer chains is denoted by f_A. Density fields of A and B blocks are described by φ_A and φ_B, respectively. The continuous density field of n_P NPs with radius R_P is given by

$$\varphi_P = \sum_{i=1}^{n_P} h(\mathbf{r}, \mathbf{r}_i) \tag{1}$$

where each NP at the spatial position $\mathbf{r}_i$ is represented by a smooth profile; that is, the density field $h(\mathbf{r},\mathbf{r}_i)$ of the ith NP smoothly transits from unity (particle region) to zero (polymer region) across a diffuse interface with thickness λ. We here use a hyperbolic function defined as $h(\mathbf{r},\mathbf{r}_i) = (1 - \tanh[(|\mathbf{r} - \mathbf{r}_i| - R_P)/\lambda])/2$. The concentration of NPs is given by $c_P = V_P/V$, where V and $V_P = \int d\mathbf{r}\varphi_P$, respectively, denote the volumes of nanocomposites and NPs. The interactions between the A and B blocks are described by the combined Flory−Huggins interaction parameter $\chi_{AB}N$. The selectivities of NPs for the A and B blocks are represented by $\chi_{AP}N$ and $\chi_{BP}N$, respectively.

Following a field-theoretical framework of polymeric fluids,[48] the free-energy functional F (in units of thermal energy k_BT) of the above system can be written as

$$F = F_{AB} + F_{PP} \tag{2}$$

The first term originates from the contributions of the free-energy functional of diblock copolymers in the nanocomposites, given by

$$\begin{aligned} F_{AB} = {} & -n_c(1 - c_P)\ln \frac{Q_{AB}}{V(1 - c_P)} \\ & + \frac{n_c}{V}\int d\mathbf{r}\Big\{ -\omega_A\varphi_A - \omega_B\varphi_B + \chi_{AB}N\varphi_A\varphi_B \\ & + \chi_{AP}N\varphi_A\varphi_P + \chi_{BP}N\varphi_B\varphi_P \\ & + \frac{1}{2}\kappa_H(\varphi_A + \varphi_B + \varphi_P - 1)^2 \Big\} \end{aligned} \tag{3}$$

where Q_{AB} represents the normalized single-chain partition function. ω_A and ω_B are the potential fields at given density fields φ_A, φ_B, and φ_P. The Helfand-type coefficient, k_H, controls the compressibility degree of nanocomposites. The second term on the right hand side of eq 2 denotes the energy contributions of interparticle interactions, expressed as[49]

$$F_{PP} = \sum_{i=1}^{n_P-1}\sum_{j>i}^{n_P}\int d\mathbf{r}h(\mathbf{r}, \mathbf{r}_i)\int d\mathbf{r}'h(\mathbf{r}', \mathbf{r}_j)u(|\mathbf{r} - \mathbf{r}'|) \tag{4}$$

where $u(|\mathbf{r} - \mathbf{r}'|)$ represents the Lennard−Jones potential of NPs.

For the nanocomposites, including the weakly compressible diblock copolymers and NPs, the evolution of the density field of the I-type component (I = A and B blocks) satisfies the Cahn−Hilliard-type equation with the local coupling Onsager coefficient[43]

$$\frac{\partial\varphi_I(\mathbf{r}, t)}{\partial t} = M_I\nabla\cdot\varphi_I(\mathbf{r})[(\mathbf{I} - \mathbf{n}_S \otimes \mathbf{n}_S\cdot\nabla\mu_I(\mathbf{r}))] + \eta_I(\mathbf{r}, t) \tag{5}$$

where M_I denotes the mobility coefficient of the I-type component, $\mathbf{I}$ is the unit tensor, $\mathbf{n}_S \equiv -\nabla\varphi_P/|\nabla\varphi_P|$ represents the local unit vector normal to the surface of NPs, $\mu_I(\mathbf{r}) \equiv \delta F/\delta\varphi_I(\mathbf{r})$ is the chemical potential of the I-type component, and η_I is the noise term. The tensor operator $\mathbf{I} - \mathbf{n}_S\otimes\mathbf{n}_S$ prevents a mass flux normal to the diffuse boundary of NPs.[50] The motion of the ith NP with mass m_i obeys Newton's equations

$$\frac{d\mathbf{r}_i}{dt} = \mathbf{v}_i \tag{6}$$

$$m_i\frac{d\mathbf{v}_i}{dt} = \int d\mathbf{r}f_i(\mathbf{r}) \tag{7}$$

where $\mathbf{v}_i$ is the velocity of the ith NP. Herein, the force $f_i(\mathbf{r})$ acting on the volume of the ith NP is decomposed into the force due to the particle−polymer and particle−particle interactions, drag and random forces expressed as[49,50]

$$f_i(\mathbf{r}) = h(\mathbf{r}, \mathbf{r}_i)(-\nabla\mu_i(\mathbf{r}) - \mathbf{v}_i/M_P - \nabla\theta_i) \tag{8}$$

where $\mu_i(\mathbf{r}) \equiv \delta F/\delta h(\mathbf{r},\mathbf{r}_i)$ is the chemical potential of the NP, M_P is the mobility coefficient of the NP, and θ_i is the Gaussian random variable.

https://dx.doi.org/10.1021/acs.macromol.0c00101
Macromolecules 2020, 53, 2111−2122

In the zone-annealing model, spatial−temporal Flory−Huggins interaction parameters $\chi_{IJ}N$ are incorporated into eq 3 of DSCFT for the mixtures of diblock copolymers and NPs. In the annealed zone with limited width w, the interaction parameters have minimum values $(\chi_{IJ}N)_{min}$. The movement of annealed zone is described by the moving velocity v. For more information about the model of zone annealing, refer to our previous works.[45−47]

This completes the description of the DSCFT/MD method for the zone-annealed nanocomposites. To elucidate the significant ordering behaviors of self-assembled nanostructures, the sizes of simulation boxes for the system of nanocomposites should be sufficiently large, leading to the much higher computational cost in the DSCFT implementations. Therefore, the numerical calculations of the DSCFT/MD method are executed in the two-dimensional boxes under the periodic boundary conditions, corresponding to the thin films of nanocomposites in the realistic experiments. Initially, the density field of NPs is calculated from eq 1 through the random placement of a fixed number of NPs in the simulation boxes. Correspondingly, the density fields φ_A and φ_B of A and B blocks are assigned. Subsequently, the procedures for numerically solving the DSCFT/MD equations are implemented as follows: (i) the evolution equations for the components of zone-annealed diblock copolymers are updated by the Crank−Nicolson method. The self-consistent determination between the density fields φ_I and potential fields ω_I in each time step of eq 5 is solved by the nonlinear conjugate gradient method. The iteration is regarded as convergence when the tolerance for the density fields becomes less than the error level of 0.01. (ii) The forces on the NPs are calculated from eq 8. The position and velocity of NPs are updated by integrating eqs 6 and 7. (iii) For the new set of NPs' positions, the DSCFT equations are updated through the above procedures. Finally, the DSCFT/MD simulations for the zone-annealed nanocomposites are stopped after 6−10 cycles of zone annealing.

In the parameter settings of the present work, the sizes of simulation boxes are set as $\sim 72.0R_g \times 72.0R_g$, which are discretized by 480 × 480 grid points. The Flory−Huggins interaction parameter of symmetric diblock copolymers (i.e., $f_A = 0.5$) is set as $\chi_{AB}N = 20.0$. The Helfand-type coefficient k_H has a value of 200 such that the deviation of the sum of $\varphi_A + \varphi_B + \varphi_P$ around 1.0 is minimized as far as possible. It is assumed that the mobility coefficients M_I of various blocks are equal. The time step for the evolution eq 5 of density fields is $\Delta t = 0.1\tau_{BCP}$, where $\tau_{BCP} \equiv \Delta x^2/M_I$ is the time unit (Δx is the discrete space). Under these selections of parameters, the diblock copolymers form the lamellae with a natural periodicity $L_0 \approx 4.0R_g$. For the parameter settings of NPs, the diffuse interface of thickness has a value of $\lambda = 0.15R_g$. The interaction parameters between the NPs and polymeric components are set as $\chi_{AP}N = 20.0$ and $\chi_{BP}N = 0$, implying that the NPs like to the B blocks. Such settings of interaction parameters can be experimentally achieved through the surface modification of NPs.[51,52] The mobility coefficient of NPs has a value of $M_P \approx 0.2M_I$.[53−56] The time step for the motion eqs 6 and 7 of NPs is $\Delta t_P = 0.02\tau_P$, where $\tau_P \equiv \Delta x^2/M_P$ is the time unit of NPs' motion. It should be mentioned that the time step Δt_P plays an important role in the self-assembly behaviors of zone-annealed nanocomposites, as shown in Figure S1 of the Supporting Information. To balance the computational cost and the numerical stability, we chose a larger time step in the DSCFT/MD simulations. In the simulations of zone annealing, the zone width is fixed at the proper value $w = 2.0L_0 \approx 8.0R_g$. For given parameter settings, each DSCFT/MD simulation is repeated 6 times with various seeds of a pseudo-random number.

3. RESULTS AND DISCUSSION

Recently, we have studied the self-assembly behaviors of pure diblock copolymers subject to zone annealing.[45−47] It was corroborated that the kinetically arrested defects of lamellae are efficiently annihilated by the introduction of the spatially and temporally dependent field. In the present work, one remarkable distinction is the incorporation of inorganic NPs, which significantly impact the ordering kinetics and the self-assembled nanostructures of nanocomposites in the realistic experiments.[57−60] In order to take the effect of NPs' incorporation into account, we carry out the DSCFT/MD simulations to explore the ordering behaviors of diblock copolymer/NP mixtures in the course of zone annealing.

In the implementation of zone-annealing simulations, the initial states are obtained from the quenching simulations of AB diblock copolymer/B-like NP composites. The quenching simulations (i.e., the zone annealing is switched off) start from a disordered state. In general, the diblock copolymers spontaneously form lamellar structures with lots of defects and the NPs are randomly dispersed in the B-rich domains (Figure 1). It should be pointed out that the long-live defects

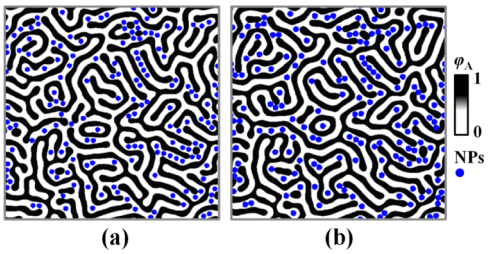

Figure 1. Self-assembled nanostructures of AB diblock copolymer/B-like NP mixtures quenched from the disordered state. (a) Simulation time $t = 4000.0\tau_{BCP}$ and (b) $t = 10\,000.0\tau_{BCP}$. Black and white colors refer to the A- and B-rich domains, respectively. The blue dots represent the NPs. The radius R_P and the concentration c_P of NPs are chosen as $0.8R_g$ and 0.06, respectively.

cannot be further annihilated in spite of an increase of the simulation time, suggesting that the defective nanostructures are kinetically trapped states due to the high energy barriers of the structural rearrangement. Such metastable nanostructures are selected as the initial states of zone-annealing simulations for the nanocomposites. Below, we apply the integrated DSCFT/MD method outlined above to investigate how zone annealing is used to program the motion of NPs and finally achieve the well-defined assemblies of NPs dispersed in the defect-free lamellae.

3.1. Diblock Copolymer/NP Mixtures Subject to Zone Annealing.

We first focus on the effect of zone annealing on the ordering behaviors of diblock copolymer/NP mixtures. The radius and concentration of NPs are chosen as $R_P = 0.8R_g$ and $c_P = 0.06$, respectively. It is assumed that the samples in the annealed zone have minimum Flory−Huggins interaction parameters $(\chi_{AB}N)_{min} = (\chi_{AP}N)_{min} = 10.0$ [designated as $(\chi N)_{min}$ below], which are slightly lower than the value of the order−disorder transition of symmetric diblock copolymers. The moving velocity v is represented by the velocity unit $\tilde{v} =$

https://dx.doi.org/10.1021/acs.macromol.0c00101
Macromolecules 2020, 53, 2111−2122

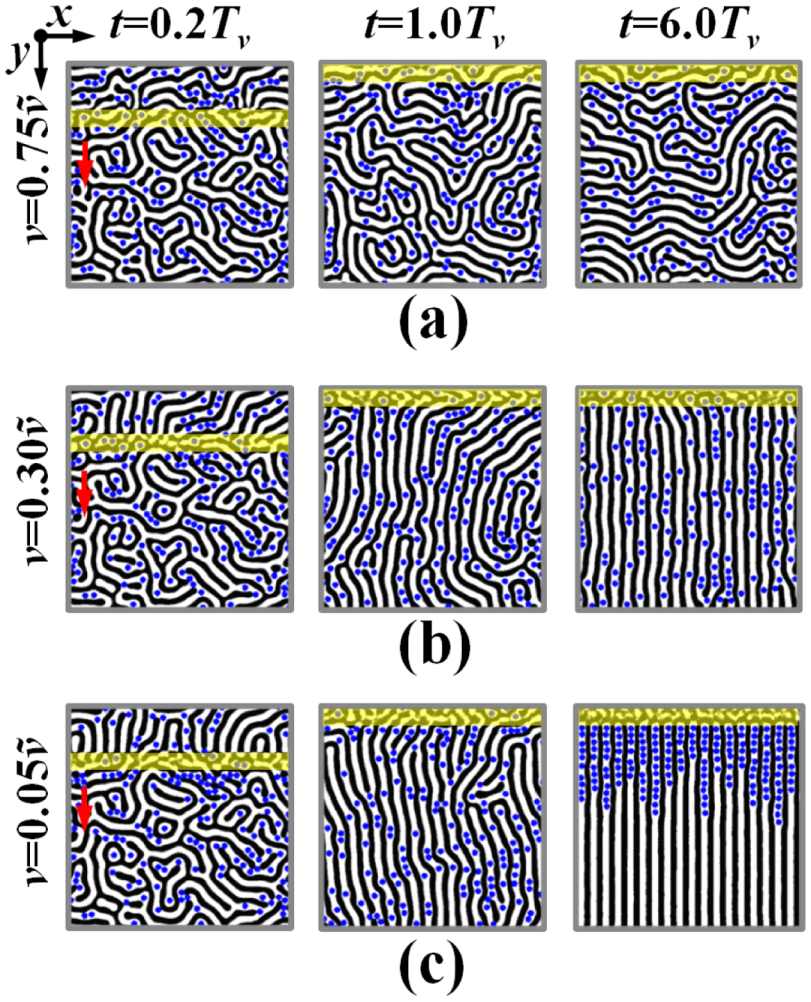

Figure 2. Morphological evolution of self-assembled nanostructures of AB diblock copolymer/B-like NP mixtures in the presence of zone annealing under various moving velocities v. (a) $v = 0.75\tilde{v}$, (b) $v = 0.30\tilde{v}$, and (c) $v = 0.05\tilde{v}$. Annealed zones highlighted by yellow color are moved periodically along the y direction from top to bottom (as marked by red arrows). The simulation times t are shown on the top of panel (a), where the periodicities T_v of zone annealing at the moving velocity $v = 0.75\tilde{v}$, $0.30\tilde{v}$, and $0.05\tilde{v}$ are, respectively, $96.0\tau_{BCP}$, $240.0\tau_{BCP}$, and $1440.0\tau_{BCP}$. The minimum Flory–Huggins interaction parameter $(\chi N)_{min}$ is set as 10.0. The radius R_p and the concentration c_p of NPs are chosen as $0.8R_g$ and 0.06, respectively. The initial states of zone-annealing simulations are obtained from the quenching cases (Figure 1b).

R_g/τ_{BCP}. The simulation time t is normalized by the periodicity $T_v = L/v$ of zone annealing, where L is the size of simulation boxes.

Figure 2 shows a series of instantaneous configurations of nanocomposites during the zone-annealing process at the moving velocity $v = 0.75\tilde{v}$, $0.30\tilde{v}$ and $0.05\tilde{v}$. After incorporating the spatially and temporally dependent field of zone annealing into DSCFT/MD simulations, a common feature in the morphological evolution of self-assembled nanostructures of nanocomposites is sketched from these snapshots. In the early stage (e.g., $t = 0.2T_v$), the defective nanostructures passed by annealed zones become unstable and the defect annihilation is evidently accelerated. After the first cycle of zone annealing (i.e., $t = 1.0T_v$), the patterns of self-assembled nanostructures become relatively ordered and the B-like NPs re-migrate into the B-rich domains to minimize the total free energy of the system. After multiple cycles of zone annealing (e.g., $t = 6.0T_v$, the annealed zones are moved to the top part of simulation boxes due to the periodic boundary conditions), the diblock copolymers re-assemble into the highly ordered lamellae, which act as scaffolds or templates to direct the spatial arrangement of B-like NPs.

More importantly, from the observations of Figure 2, one can deduce a significant outcome that the final morphology of nanocomposites and the spatial arrangement of NPs are in close relation with the moving velocity of zone annealing. In the case of a larger value of the moving velocity (e.g., $v = 0.75\tilde{v}$), a number of grain boundaries of lamellae remain in the patterns, and the spatial arrangement of NPs in the B-rich domains is still random (Figure 2a). As the moving velocity v is reduced to $0.30\tilde{v}$, the diblock copolymers re-organize into the highly ordered lamellae due to the annihilations of defects (Figure 2b). The favorable wetting interactions between the NPs and the B blocks cause the NPs to be preferentially localized in the straight B-rich domains of well-ordered lamellae, but their spatial arrangement is still random. With a further decrease of moving velocity (e.g., $v = 0.05\tilde{v}$), the NPs are driven to re-organize into long chains located in the front of the annealed zone (Figure 2c). As shown in Figure S2 of the Supporting Information, these behaviors are also observed for the system of asymmetric diblock copolymer/NP mixtures. These theoretical predictions manifest the fact that the zone annealing can manipulate both the ordering degree of self-assembled nanostructures and the spatial arrangement of NPs

https://dx.doi.org/10.1021/acs.macromol.0c00101
Macromolecules 2020, 53, 2111−2122

in the B-rich domains through finely tuning the moving velocity.

To quantify the ordering degree of self-assembled nanopatterns, the order parameter β of the lamellae along the pathway of zone annealing (i.e., the y direction in the present work) is introduced[61,62]

$$\beta(t) = \langle\langle\phi(\mathbf{r}, t)_y^2/\phi(\mathbf{r}, t)^2\rangle_y\rangle_x \quad (9)$$

where $\phi(\mathbf{r},t) \equiv \varphi_A(\mathbf{r},t) - \varphi_B(\mathbf{r},t)$ is the difference of density fields between the A and B blocks. The brackets $\langle\cdot\rangle_\gamma$ ($\gamma = x$ and y) stand for the average along the γ direction. Here, $\beta = 1.0$ corresponds to the defect-free lamellae along the annealing direction, while $\beta \to 0$ suggests the defective lamellae with multiple orientations. It should be mentioned that β has an upper limit value around 0.8 due to the weak segregation of diblock copolymers in the annealed zone.

Figure 3a shows the order parameter β of lamellae in terms of the time under various moving velocities v. Through the

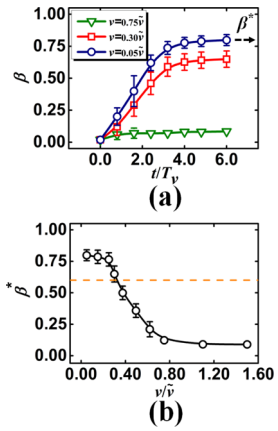

Figure 3. (a) Temporal evolution of order parameter β of lamellar nanostructures subject to zone annealing at moving velocity $v = 0.75\tilde{v}$, $0.30\tilde{v}$, and $0.05\tilde{v}$. (b) Steady-order parameter β^* of lamellar nanostructures in terms of the moving velocity. The dashed line highlights the critical value of the steady-order parameter. In panels (a,b), each data point is averaged over six independent runs. The error bars are shown only when the standard deviations are larger than the height of symbols.

introduction of zone annealing into the nanocomposites, the order parameter of self-assembled nanostructures increases during the few cycles of zone annealing due to the defect annihilation. However, there are some remarkable differences for the order parameters of nanostructures in the final stage of zone-annealing simulations. Under the condition of $v = 0.75\tilde{v}$, the order parameter exhibits a low value, implying that the lamellae remain the defective state in spite of the introduction of zone annealing. However, for the moving velocities of $0.30\tilde{v}$ and $0.05\tilde{v}$, their order parameters gradually increase and finally reach larger values, suggesting that the defective lamellae transit to the well-ordered nanostructures.

The steady-order parameter β^* is used to evaluate the efficiency of zone annealing. As highlighted in Figure 3a, the plateau value of the order parameter is regarded as parameter β^*. Figure 3b depicts the steady-order parameter β^* in terms of the moving velocity v. As the annealed zone is slowly moved, the time of diblock copolymers staying in the annealed zone becomes long and the polymer molecules have the opportunity to re-organize themselves; hence, the long-live defects can be removed and the well-ordered nanostructures are finally achieved. In particular, under the condition of $v \le 0.30\tilde{v}$, the metastable defects are annihilated by the spatially localized, mobile field of zone annealing, and the value of parameter β^* is larger than 0.60 (highlighted by the dashed line in Figure 3b), suggesting that zone annealing with the small value of the moving velocity is sufficient to overcome the energy barriers and results in the formation of defect-free nanostructures of nanocomposites.

In order to elucidate the spatial arrangement of NPs in the course of zone annealing, their motion is quantified by the normalized position displacement $\Delta\hat{r}$ given by[63,64]

$$\Delta\hat{r} = \frac{1}{n_p v \Delta T}\sum_{i=1}^{n_p}|\Delta\mathbf{r}_i| \quad (10)$$

where $|\Delta\mathbf{r}_i|$ represents the displacement of the ith NP over a time interval (e.g., $\Delta T = 0.25T_v$) and $v\Delta T$ represents the moving distance of the annealed zone. If $\Delta\hat{r} \approx 1$, the NPs are driven to directionally move along the pathway of the annealed zone, indicating a strong coupling between NPs and zone annealing. If $\Delta\hat{r} \to 0$, the NPs display a random motion, indicating a weak coupling.

Figure 4a depicts the normalized displacement $\Delta\hat{r}$ of NPs in terms of the time. For the moving velocity $v = 0.05\tilde{v}$, after

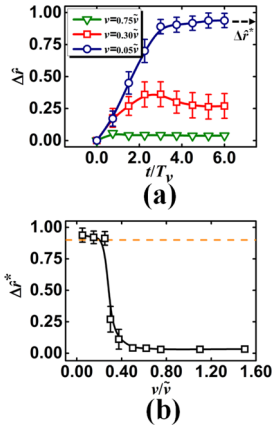

Figure 4. (a) Temporal evolution of the normalized displacement $\Delta\hat{r}$ of NPs subject to zone annealing at the moving velocity $v = 0.75\tilde{v}$, $0.30\tilde{v}$, and $0.05\tilde{v}$. (b) Steady normalized displacement $\Delta\hat{r}^*$ of NPs in terms of the moving velocity v. The dashed line highlights the critical value of the steady normalized displacement.

several cycles of zone annealing, $\Delta\hat{r}$ reaches a large value around 0.92, implying that almost all the NPs directionally move along the pathway of the annealing zone. However, different behaviors of NPs are observed in the cases of the moving velocities of $0.75\tilde{v}$ and $0.30\tilde{v}$. Under the condition of $v = 0.75\tilde{v}$, the NPs randomly move during the entire annealing process, as evidenced by a small value of $\Delta\hat{r}$. For the moving velocity $v = 0.30\tilde{v}$, $\Delta\hat{r}$ maintains an intermediate value, implying that these NPs undergo a finite displacement only along the pathway of the annealing zone. In other words, the directional motion of NPs cannot be triggered by zone annealing with a fast moving velocity.

Figure 4b plots the steady normalized displacement $\Delta\hat{r}^*$ of NPs in terms of the moving velocity. This quantity is schematically illustrated in Figure 4a. In the case of $v \le 0.30\tilde{v}$, the steady normalized displacement is larger than 0.9,

https://dx.doi.org/10.1021/acs.macromol.0c00101
Macromolecules 2020, 53, 2111−2122

implying that the chain-like assemblies of NPs are directionally moved along the pathway of the annealed zone. As the moving velocity is beyond the range (i.e., $v > 0.30\tilde{v}$), the steady normalized displacement shows a notable decrease, suggesting that the NPs randomly move in the B-rich domains. Therefore, from the observations of Figures 2−4, it is definitely demonstrated that zone annealing can efficiently annihilate the long-live defects to yield well-ordered nanostructures as well as induce the directional motion of NPs to achieve the well-defined assemblies.

In order to comprehend how zone annealing impacts the motion and arrangement of NPs in the self-assembled nanostructures, we take a closer look at the dynamic trajectories of the structural evolution by considering the microscopic details. Figure 5 illustrates the three-dimensional

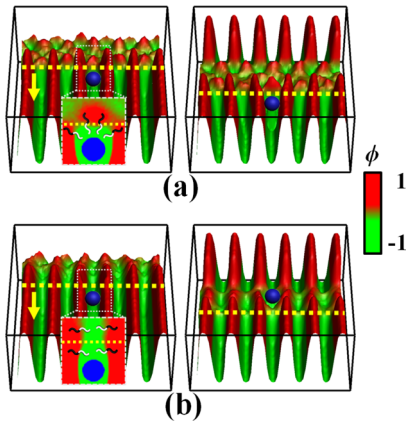

Figure 5. Three-dimensional height maps of density distribution $\phi(\mathbf{r},t) \equiv \varphi_A(\mathbf{r},t) - \varphi_B(\mathbf{r},t)$ for the moving velocity (a) $v = 0.05\tilde{v}$ and (b) $v = 0.75\tilde{v}$. The minimum Flory−Huggins interaction parameter is fixed at $(\chi N)_{min} = 10.0$. Images show a portion of the simulation boxes. Left and right panels correspond to the early and later stages as the annealed zone passes over the samples. The fronts of annealed zone are highlighted by the dashed lines. Insets illustrate the self-assembled nanostructures of nanocomposites enclosed by the dotted line boxes and the corresponding configurations of diblock copolymer chains.

height maps for the difference $\phi(\mathbf{r},t) \equiv \varphi_A(\mathbf{r},t) - \varphi_B(\mathbf{r},t)$ of density fields between the A and B components. For clarity, a part of the simulation boxes is shown in the high-contrast images, where only a single NP is located in the B-rich domain of the defect-free lamellae. As the annealed zone is moved slowly (Figure 5a), the molecule chains of diblock copolymers have sufficient time to respond to the environmental change in the annealed zone; hence, the difference of density fields in the annealed zone (i.e., disordered domains) is smaller than that in the rest of samples. At the front of the annealed zone, a sequence of half-period shifts are witnessed to connect the transition from the lamellae to the disordered domains (i.e., response layer), originating from the combination of the incompatibility of distinct blocks and the topology of copolymer chains.[12,65] That is, the high-density distribution of A blocks in the response layer lies between the distinct lamellae (highlighted by the dotted line box in Figure 5a). These observations of density distribution in the response layer are also identified by the dynamic field theory simulations for the solvent evaporation of diblock copolymers.[66] Such A-rich domains in the response layer exert a repulsive force on the B-like NP (inset of Figure 5a), which arises from their incompatibility. The repulsive force pushes the NP to directionally move along the pathway of the annealed zone. As the annealed zone continues to be moved over the sample, the above scenarios are repeated. As a result, the front of the annealed zone effectively collects a number of NPs after several cycles of zone annealing. However, as the annealed zone is moved fast, the copolymer chains do not have sufficient time to re-organize themselves at the front of the annealed zone (Figure 5b). In other words, the observation of the response layer is unobvious in the annealed zone under this condition. Consequently, the repulsive force described above is weak, and the movement of NPs in the B-rich domains is mainly driven by the Brownian motion, leading to the formation of randomly dispersed NPs.

It is helpful to compare the dynamic trajectories of NPs dispersed in the homopolymer blends and diblock copolymers subject to zone annealing. As shown in Figure S3 of the Supporting Information, the response layers cannot be identified in the annealed zone of homopolymer blends, and the NPs cannot be collected by the annealed zone in spite of the slow moving velocity. It is further demonstrated that the response layers originating from the chain topology of diblock copolymers allow the NPs to directionally move and finally achieve the chain-like assemblies dispersed in the energetically favorable domains.

3.2. Effect of the Interaction Parameter of Zone Annealing. The minimum Flory−Huggins interaction parameter $(\chi N)_{min}$ of zone annealing is a significant factor that impacts the self-assembly behaviors of nanocomposites, which are depicted in Figure 6. The moving velocity of the

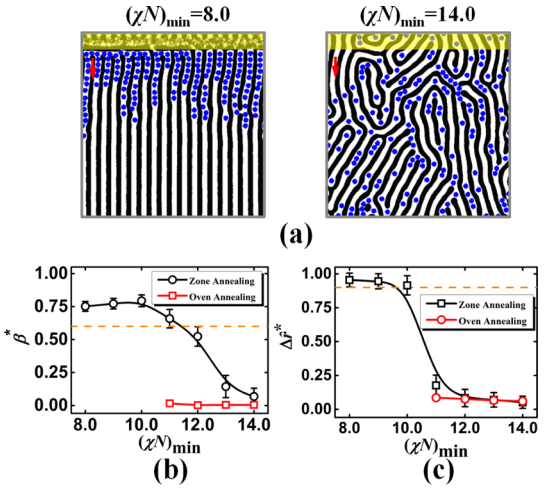

Figure 6. Effect of the minimum Flory−Huggins interaction parameter $(\chi N)_{min}$ of the annealed zone on the self-assembly behaviors of nanocomposites. (a) Morphologies of self-assembled nanostructures in the final stage of zone annealing simulations. (b) Steady-order parameter β^* and (c) steady normalized displacement $\Delta\hat{r}^*$ in terms of the Flory−Huggins interaction parameter $(\chi N)_{min}$ for the nanocomposites subject to zone and oven annealing. The moving velocity v of the annealed zone is fixed at $0.15\tilde{v}$.

annealed zone is fixed at $v = 0.15\tilde{v}$. When the minimum Flory−Huggins parameter is below the value of the order−disorder transition [i.e., $(\chi N)_{min} < 10.5$], the self-assembled nanostructures of diblock copolymers display a high ordering degree and the NPs are driven to form the chain-like assemblies in the front of the annealed zone, evidenced by the larger values of β^*

https://dx.doi.org/10.1021/acs.macromol.0c00101
Macromolecules 2020, 53, 2111−2122

and $\Delta\hat{r}^*$. However, with an increase of $(\chi N)_{min}$, both β^* and $\Delta\hat{r}^*$ approach zero. In this case, the self-assembled nanostructures present multiple orientations and the NPs exhibit a random dispersion in the B-rich domains of the defective lamellae. Such ordering behaviors of nanocomposites can be also understood by the response layers of diblock copolymers (Figure S4 of the Supporting Information).

We also compare the self-assembly behaviors of diblock copolymer/NP mixtures subject to zone and oven annealing. The simulations of oven annealing start from the defective nanostructures shown in Figure 1b, and the Flory–Huggins interaction parameters are set as $(\chi N)_{min}$ in the entire boxes. As shown in Figure S5 of the Supporting Information, some of the defects are removed by oven annealing, but the grain boundaries of the lamellae remain in the patterns. The steady-order parameter β^* and normalized displacement $\Delta\hat{r}^*$ have small values (Figure 6b,c), indicating the observations of the defective lamellae and randomly dispersed NPs in the case of oven annealing.

As illustrated above, the design parameters of zone annealing [i.e., the moving velocity v and the minimum Flory–Huggins interaction parameter $(\chi N)_{min}$] play vital roles in impacting the self-assembly behaviors of nanocomposites. We carry out a series of DSCFT/MD simulations for the zone-annealed nanocomposites, which allow us to construct the steady-order parameter β^* and the normalized displacement $\Delta\hat{r}^*$ landscapes plotted by the colorful contour maps in the v–$(\chi N)_{min}$ plane (Figure 7). In light of how the steady-order parameter β^* and the normalized displacement $\Delta\hat{r}^*$ are affected by the moving velocity v and the minimum Flory–Huggins interaction parameter $(\chi N)_{min}$, the maps are respectively divided into two characteristic regions, which are approximately separated by the solid lines. Under the conditions of large values of moving velocity and interaction parameters, the zone-annealed nanocomposites form the defective lamellae filled with the random distribution of NPs. With a decrease of the values of moving velocity and interaction parameter, the diblock copolymers are directed to re-organize into the well-ordered lamellae, and the NPs are programmed to form the long chains. It should be mentioned that the critical moving velocity for the boundaries between the two characteristics regions is decreased exponentially with an increase of interaction parameter, suggesting that the design parameters of zone annealing are significant factors to rationally construct the multifunctional nanodevices with well-ordered nanostructures and well-defined NPs.

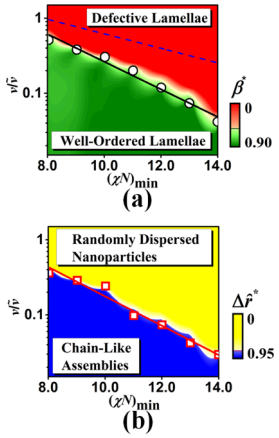

Figure 7. Contour maps about (a) steady-order parameter β^* and (b) steady normalized displacement $\Delta\hat{r}^*$ in the plane of moving velocity $v/\tilde{v}$ and the minimum Flory–Huggins interaction parameter $(\chi N)_{min}$. In panel (a), the solid line divides the contour map of lamellar nanostructures into two regions: well-ordered and defective lamellae. The dashed line highlights the boundary for the pure diblock copolymers. In panel (b), the solid line divides the contour map of NPs' arrangement into two regions: chain-like assemblies and randomly dispersed NPs. The color bars present the code for the values of β^* and $\Delta\hat{r}^*$. Note that the vertical axis has a logarithmic scale.

In particular, the dashed line of Figure 7a represents the boundary between the well-ordered and defective nanostructures for the system of pure diblock copolymers. Similarly, the spatial regularity of the lamellae depends strongly on the moving velocity and the minimum Flory–Huggins interaction parameter. However, in comparison with the case of nanocomposites, the characteristic region of well-ordered nanostructures is enlarged due to the removal of NPs.

Another salient feature for the nanocomposites is that the chain-like assemblies of NPs are achieved during the process of zone annealing, which is highlighted by the red line in Figure 7b. It is worthwhile pointing out that the location of the red line is lower than that of the black line (corresponding to the critical moving velocity of the defect-free lamellae in Figure 7a) at given values of $(\chi N)_{min}$. This observation manifests the fact that the chain-like assemblies of NPs form after the ordering of lamellar nanostructures in the course of zone annealing.

To further testify the validation of zone annealing for the unique self-assembly behaviors of nanocomposites, we also perform additional simulations for the diblock copolymer/NP mixtures, which start from the homogeneous states and quench into the microphase-separated state (Figure S6 of the Supporting Information). Meanwhile, the annealed zone is periodically moved from the top to bottom of samples. It is found that the ordering degree of lamellar nanostructures and the spatial arrangement of NPs in the late stage of zone annealing simulations are identical to those in the case of initial configurations of defective nanostructures (Figure 2), revealing that the self-assembly behaviors of nanocomposites are less susceptible to the initial states.

3.3. Effects of Physicochemical Properties of NPs. In this subsection, we investigate the effects of physicochemical properties of NPs on the self-assembly behaviors of zone-annealed nanocomposites. The minimum Flory–Huggins interaction parameter $(\chi N)_{min}$ in the annealed zones is chosen as 10.0. Below, we use our developed DSCFT/MD method to investigate the ordering behaviors of nanocomposites in terms of the concentration and radius of NPs.

Figures 8 and S7 of the Supporting Information display the effect of concentration c_p of NPs on the ordering behaviors of zone-annealed nanocomposites. The moving velocity is set as $v = 0.15\tilde{v}$. The radius of NPs is fixed at $R_p = 0.8R_g$. When the concentration c_p of NPs is low (e.g., $c_p = 0.02$), the well-ordered lamellae and well-defined assemblies of NPs are achieved due to the relatively weak steric hindrance among NPs, as evidenced by the larger values of $\Delta\hat{r}^*$ and β^*. As the concentration of NPs is increased (e.g., $c_p = 0.12$), the NPs in the B-rich domains become crowded, leading to an enhancement of the steric hindrance among neighboring NPs. In particular, a portion of NPs prefer to accumulate in the front of the annealed zone (Figure 8a), causing the swelling of domains near this zone. In the rest of the NP-filled sample, the lamellae

https://dx.doi.org/10.1021/acs.macromol.0c00101
Macromolecules 2020, 53, 2111–2122

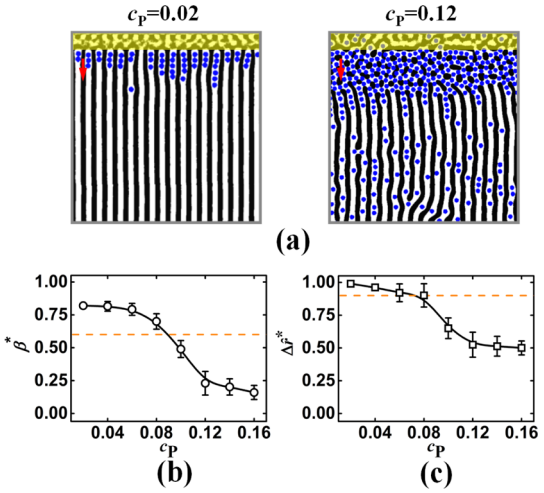

Figure 8. Effect of NPs' concentration c_P on ordering behaviors of zone-annealed nanocomposites. (a) Morphologies of self-assembled nanostructures in the final stage of zone annealing simulations. (b) Steady-order parameter β^* and (c) steady normalized displacement $\Delta\hat{r}^*$ as a function of the NPs' concentration c_P. The moving velocity and the minimum Flory−Huggins interaction parameter are set as $v = 0.15\tilde{v}$ and $(\chi N)_{min} = 10.0$, respectively.

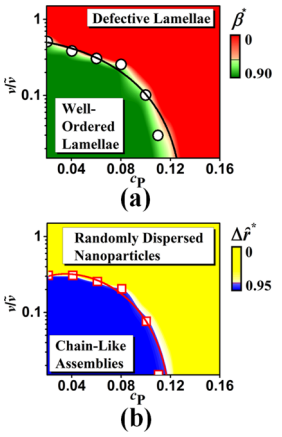

Figure 9. Contour maps about (a) steady-order parameter β^* and (b) steady normalized displacement $\Delta\hat{r}^*$ in the plane of moving velocity $v/\tilde{v}$ and NPs' concentration c_P. The minimum Flory−Huggins interaction parameter and NPs' radius are chosen as $(\chi N)_{min} = 10.0$ and $R_P = 0.8R_g$, respectively.

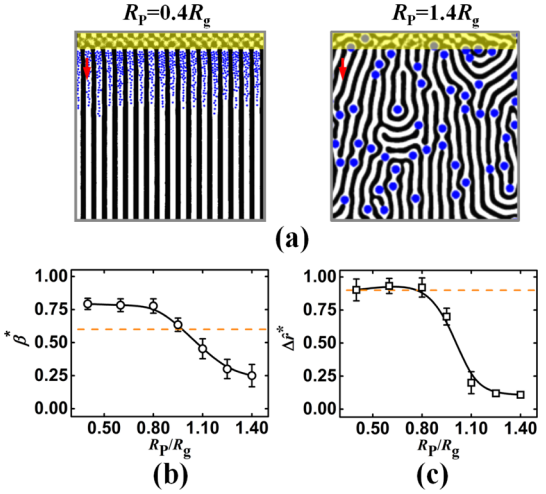

Figure 10. Effect of NPs' radius R_P on ordering behaviors of diblock copolymer/NP mixtures subject to zone annealing. (a) Morphologies of self-assembled nanostructures. (b) Steady-order parameter β^* and (c) steady normalized displacement $\Delta\hat{r}^*$ as a function of NPs' radius R_P. The moving velocity and the minimum Flory−Huggins interaction parameter are set as $v = 0.15\tilde{v}$ and $(\chi N)_{min} = 10.0$, respectively.

display some degree of ordering due to the defect annihilation with the help of zone annealing, but the spatial arrangement of NPs in the B-rich domains is random. Between the swelling and ordering areas of self-assembled nanostructures, the defects cannot be eliminated by the repeated annealing due to the inhomogeneous swelling of lamellar nanostructures.[67] As a result, an increase of c_P results in the lower magnitudes of β^* and $\Delta\hat{r}^*$, which are respectively demonstrated in Figure 8b,c.

In order to capture the effects of concentration c_P of NPs and moving velocity v of zone annealing on the ordering behaviors of zone-annealed nanocomposites, we calculate the steady-order parameter β^* of the lamellae and the normalized displacement $\Delta\hat{r}^*$ of NPs as functions of c_P and v. These allow us to construct the β^* and $\Delta\hat{r}^*$ landscapes presented by the contour maps in the $v-c_P$ plane, which are respectively depicted in Figure 9a,b. The characteristic regions are divided by the solid lines. When c_P is smaller than 0.12, well-ordered lamellae and chain-like assemblies are achieved by tuning the moving velocity of zone annealing. However, an increase of concentration of NPs prevents the formation of well-ordered nanostructures in spite of the incorporation of zone annealing. For instance, the nanocomposites with $c_P = 0.11$ self-assemble into the well-ordered nanostructures at the lower moving velocity by about 10 cycles of zone annealing. As the concentration c_P of NPs is increased to $c_P = 0.16$, the entire sample consists of the mixed phases of lamellae and cylinders, and the zone annealing no longer introduces a noticeable ordering into the system of nanocomposites.

We now turn our attention to the effect of NPs' radius R_P on the self-assembly behaviors of zone-annealed nanocomposites (Figure S8 of the Supporting Information). The concentration of NPs is fixed at $c_P = 0.06$. As shown in Figure 10, for a given moving velocity $v = 0.15\tilde{v}$, smaller NPs (e.g., $R_P \leq 0.75R_g$) result in the highly ordered lamellae and their better arrangement. When the size of NPs (i.e., NP diameter $D_P = 2.0R_P$) becomes comparable to the half-domain width of the lamellae (i.e., $L_0/2$, where $L_0 \approx 4.0R_g$), the interfaces of distinct domains of diblock copolymers are distorted by the larger NPs. The phenomenon results in the consequent loss of the ordering degree of lamellae, corresponding to a decrease of the steady-order parameter β^*. Simultaneously, an increase of the NP size leads to a decrease of the steady normalized displacement $\Delta\hat{r}^*$, reflecting the random dispersion of NPs in the entire sample.

Figure 11 shows the landscapes of the steady-order parameter β^* of the lamellae and the normalized displacement $\Delta\hat{r}^*$ of NPs presented by the contour maps in the $v-R_P$ plane. Under the condition of small NPs' radius (e.g., $R_P \leq L_0/4$), the nanocomposites can successfully escape the kinetically trapped states with the help of zone annealing and reach the well-ordered nanostructures with defect-free lamellae and well-defined assemblies of NPs. Meanwhile, the critical moving velocity to yield the well-ordered nanostructures has a tight relation with the radius of NPs. Beyond this range (i.e., $R_P >$

https://dx.doi.org/10.1021/acs.macromol.0c00101
Macromolecules 2020, 53, 2111−2122

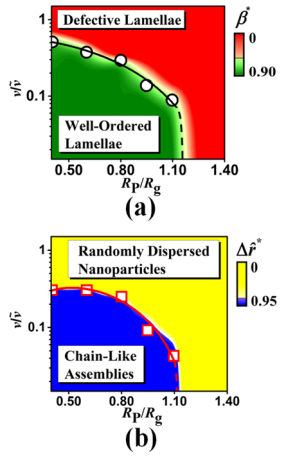

Figure 11. Contour maps about (a) steady-order parameter β^* and (b) steady normalized displacement $\Delta\hat{r}^*$ in the plane of moving velocity $v/\tilde{v}$ and NPs' radius R_P. The dashed lines are the estimated transition boundaries. The NPs' concentration c_P is fixed at 0.06.

$L_0/4$), the defective lamellae of zone-annealed nanocomposites are observed, because the local interfaces of microphase-separated structures are strongly distorted by the larger NPs.

3.4. Experimental Discussion. The zone-annealed nanocomposites demonstrated by the DSCFT/MD simulations can be realized in the experimental researches, and the predicted results are corroborated by the experimental analyses. For instance, Karim's group has recently adapted the zone-annealing procedure to order the hybrid materials of cylinder-forming diblock copolymers filled with gold NPs.[29,30] As evidenced by the grazing-incidence small-angle X-ray scattering and atom force microscopy, the ordering degree of cylinders can be notably enhanced by the incorporation of zone annealing, and the corresponding orientation is tuned by the loading of NPs. While the specifics of diblock copolymers in the experimental system are different from those presented here, there are some fundamental similarities in the self-assembly behaviors of nanocomposites. That is, in the presence of zone annealing, the diblock copolymers filled with NPs are guided to re-assemble into the highly ordered nanostructures, as demonstrated in Figures 2 and 3. Meanwhile, the addition of NPs significantly impacts the self-assembled nanostructures of diblock copolymers subject to zone annealing (Figure 8). These findings obtained from DSCFT/MD simulations are in accordance with the experimental results of zone-annealed nanocomposites. Therefore, this system could provide an ideal starting point for introducing the inorganic NPs into the organic matrix and kinetically controlling the ordering degree of self-assembled nanostructures of nanocomposites.

Furthermore, the spatially localized, mobile field of zone annealing in conjunction with the scaffolds of diblock copolymers provides the driving force (i.e., the response layers of diblock copolymers) to create the moving fronts, which are ultimately used to program the directional motion of NPs in the energetically favorable domains (Figure 5). Such intriguing phenomenon originates from the complex cooperative interactions in the system, including the preferential wetting interaction between the NPs and one of the blocks, steric repulsion between the NPs, and the response of diblock copolymers to zone annealing. As a result, zone annealing for the diblock copolymer/NP mixtures plays an important role in manipulating the spatial arrangement of inorganic NPs in the organic matrix. Specifically, by varying the moving velocity and the minimum Flory−Huggins interaction of zone annealing, the spatial arrangement of dispersed NPs can be categorized into two distinct states: randomly dispersed NPs and chain-like assemblies of NPs (Figure 7). The appearance of chain-like assemblies, where the NPs are sequestered in the front of zone annealing and moved with zone annealing, provides a powerful means of delivering the NPs to a particular location in the polymeric matrix. Once the zone-annealed nanocomposites are quenched, the desired nanostructures with well-defined assemblies of NPs are locked into the hybrid materials, which will display the strongly collective optical and electric properties in comparison with the poor organization of NPs within the scaffolds.

Zone annealing for the nanocomposites can be also utilized to construct the banded assemblies of NPs with the help of the response layers of diblock copolymers. Figure 12a schematically illustrates the movement protocol (including the forward and backward-and-forward modes) of the annealed zone in DSCFT/MD simulations. To ensure the entrance of annealing fronts into the assemblies of NPs ($t = 0$ in Figure 12b) and the pre-formation of the first well-defined layer of NPs ($t = t_1$ in Figure 12b), the annealed zone is moved at velocity $v > v_c$ (v_c is the critical velocity to yield chain-like assemblies as shown in Figure 7b) and the forward velocity $v_f < v_c$, respectively. The representative nanostructures ($t = t_1$ in Figure 12b) are selected as the initial configurations of zone-annealing simulations in the backward-and-forward mode. The annealed zone is moved along the y direction at the forward velocity v_f and subsequently moved along the $-y$ direction at the backward velocity $v_b = -v_f$, respectively. The movement periodicity of the annealed zone is given by $T_{ZA} \equiv 2w/v_f$, where w is the width of zone annealing. The DSCFT/MD simulations for the backward-and-forward movement of zone annealing are stopped after 3 cycles. Figure 12c shows the self-assembled nanostructures of nanocomposites subject to the backward-and-forward mode of zone annealing under various moving velocities. When the moving velocities are set as v_f =

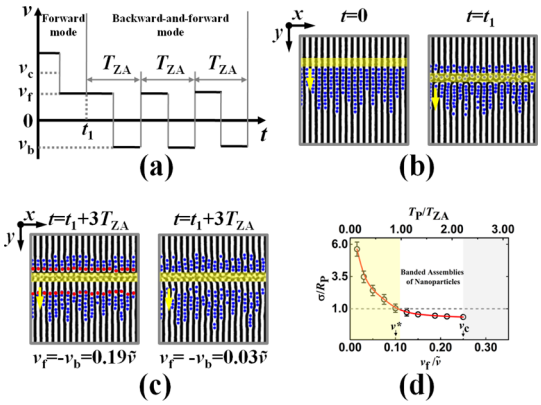

Figure 12. (a) Schematic illustration of the movement protocol of the annealed zone. (b) Self-assembled nanostructures of nanocomposites in the forward mode of zone annealing at time $t = 0$ and t_1. (c) Self-assembled nanostructures of nanocomposites in the backward-and-forward mode of zone annealing at time $t = t_1 + 3T_{ZA}$ under various moving velocities. (d) Standard deviation of NPs' positions in terms of the moving velocities. The radius and concentration of NPs are chosen as $R_P = 0.8R_g$ and $c_P = 0.06$, respectively.

https://dx.doi.org/10.1021/acs.macromol.0c00101
Macromolecules 2020, 53, 2111−2122

$-v_b = 0.19\tilde{v}$, the NPs at the front of assemblies (highlighted by red dots) form the well-defined layers (i.e., banded assemblies of NPs). As the moving velocities are decreased to $v_f = -v_b = 0.03\tilde{v}$, the NPs at the front of assemblies have a larger displacements in the y direction due to their longtime Brownian motion.

To elucidate the spatial arrangement of NPs in the front of assemblies, the displacement is quantified by the standard deviation of NPs' positions given by $\sigma \equiv \left(\sum_{i=1}^{n_L} (y_i - \bar{y})^2 / n_L\right)^{1/2}$, where n_L is the number of NPs and $\bar{y}$ is the average value of the vertical position y_i. Under the condition of $\sigma < R_P$, the NPs in the front of assemblies are regarded as the formation of well-defined layers and the achievement of banded assemblies. Figure 12d depicts the standard deviation of NPs' positions in terms of the moving velocities of zone annealing. As the moving velocities $v_f = -v_b$ are larger than the lower critical value $v^* \approx 0.10\tilde{v}$, the standard deviation of NPs' positions is smaller than the value of R_P, implying the achievement of banded assemblies. It should be noted that the moving velocities of zone annealing must be smaller than the upper critical velocity $v_c \approx 0.25\tilde{v}$ to ensure the directional motion of NPs.

The spatial arrangement of NPs in the zone-annealed nanocomposites can be understood by the competition between two important time scales, T_{ZA} and T_P. $T_{ZA} \equiv 2w/v_f = 16\tau_{BCP}/(v_f/\tilde{v})$ is the time scale of zone annealing in the backward-and-forward mode. T_P is the diffusion time scale of NPs and can be roughly estimated as $T_P \equiv R_P^2/M_P \approx 142\tau_{BCP}$. As $T_P/T_{ZA} > 1$, corresponding to the estimated value $v_f > 0.11\tilde{v} \approx v^*$, the displacement of NPs does not exceed the radius of NPs, resulting in the formation of banded assemblies. These results provide significant information for the experimentalists to rationally construct the banded assemblies of NPs by carefully designing the backward-and-forward mode of zone annealing.

It should be mentioned that our DSCFT/MD simulations are implemented in the two-dimensional space to reduce the computational costs for the numerical solutions of modified diffusion equations in the inversion problems of local density fields of diblock copolymers. The two-dimensional simulations do not take into account the effect of film thickness, which plays an important role in the ordering process of self-assembled nanostructures, especially for the system of asymmetric diblock copolymers (Figure S2 of the Supporting Information). With the help of accelerating techniques based on the graphics-processing units,[47,68] one can overcome the computational intensity of DSCFT/MD simulations and thoroughly study the self-assembly behaviors of zone-annealed nanocomposites, such as the effect of film thickness and the ordering process of asymmetric diblock copolymer/NP mixtures, the orientation change of nanostructures induced by the introduction of NPs, and the morphological transition of self-assembled nanostructures via zone annealing.

4. CONCLUSIONS

A new computational model, integrating DSCFT and MDs, is developed and used to investigate the ordering behaviors of hybrid diblock copolymer/NP mixtures in the presence of zone annealing. The integrated model enables us to analyze the structural evolution of self-assembled patterns and the motion of NPs. Using the simulations, we corroborate the findings that the well-ordered nanostructures are achieved by virtue of zone annealing. Because of the directional motion of NPs originating from the presence of response layers of diblock copolymers, the NPs are programmed to form the chain-like assemblies in the front of the annealed zone. The simulations also reveal the importance of parameter choices of zone annealing and the NPs to achieve the well-ordered nanostructures of diblock copolymer/NP mixtures and the well-defined assemblies of NPs dispersed in the polymeric matrix.

■ ASSOCIATED CONTENT

Supporting Information

The Supporting Information is available free of charge at https://pubs.acs.org/doi/10.1021/acs.macromol.0c00101.

Additional simulation results (PDF)

■ AUTHOR INFORMATION

Corresponding Authors

Liangshun Zhang − *Shanghai Key Laboratory of Advanced Polymeric Materials, Key Laboratory for Ultrafine Materials of Ministry of Education, School of Materials Science and Engineering, East China University of Science and Technology, Shanghai 200237, China;* orcid.org/0000-0002-0182-7486; Email: zhangls@ecust.edu.cn

Jiaping Lin − *Shanghai Key Laboratory of Advanced Polymeric Materials, Key Laboratory for Ultrafine Materials of Ministry of Education, School of Materials Science and Engineering, East China University of Science and Technology, Shanghai 200237, China;* orcid.org/0000-0001-9633-4483; Email: jlin@ecust.edu.cn

Authors

Jiabin Gu − *Shanghai Key Laboratory of Advanced Polymeric Materials, Key Laboratory for Ultrafine Materials of Ministry of Education, School of Materials Science and Engineering, East China University of Science and Technology, Shanghai 200237, China*

Runrong Zhang − *Shanghai Key Laboratory of Advanced Polymeric Materials, Key Laboratory for Ultrafine Materials of Ministry of Education, School of Materials Science and Engineering, East China University of Science and Technology, Shanghai 200237, China*

Complete contact information is available at: https://pubs.acs.org/10.1021/acs.macromol.0c00101

Notes

The authors declare no competing financial interest.

■ ACKNOWLEDGMENTS

This work was supported by the National Natural Science Foundation of China (21574040, 21873029, 51833003, 51621002, and 21975073).

■ REFERENCES

(1) Pileni, M.-P. Self-Assembly of Inorganic Nanocrystals: Fabrication and Collective Intrinsic Properties. *Acc. Chem. Res.* **2007**, *40*, 685−693.

(2) Nie, Z.; Petukhova, A.; Kumacheva, E. Properties and Emerging Applications of Self-Assembled Structures Made from Inorganic Nanoparticles. *Nat. Nanotechnol.* **2010**, *5*, 15−25.

(3) Ross, M. B.; Mirkin, C. A.; Schatz, G. C. Optical Properties of One-, Two-, and Three-Dimensional Arrays of Plasmonic Nanostructures. *J. Phys. Chem. C* **2016**, *120*, 816−830.

(4) Wang, D.; Guan, J.; Hu, J.; Bourgeois, M. R.; Odom, T. W. Manipulating Light−Matter Interactions in Plasmonic Nanoparticle Lattices. *Acc. Chem. Res.* **2019**, *52*, 2997−3007.
(5) Kuzyk, A.; Schreiber, R.; Fan, Z.; Pardatscher, G.; Roller, E.-M.; Högele, A.; Simmel, F. C.; Govorov, A. O.; Liedl, T. DNA-Based Self-Assembly of Chiral Plasmonic Nanostructures with Tailored Optical Response. *Nature* **2012**, *483*, 311−314.
(6) Heuer-Jungemann, A.; Feliu, N.; Bakaimi, I.; Hamaly, M.; Alkilany, A.; Chakraborty, I.; Masood, A.; Casula, M. F.; Kostopoulou, A.; Oh, E.; Susumu, K.; Stewart, M. H.; Medintz, I. L.; Stratakis, E.; Parak, W. J.; Kanaras, A. G. The Role of Ligands in the Chemical Synthesis and Applications of Inorganic Nanoparticles. *Chem. Rev.* **2019**, *119*, 4819−4880.
(7) Dujardin, E.; Peet, C.; Stubbs, G.; Culver, J. N.; Mann, S. Organization of Metallic Nanoparticles Using Tobacco Mosaic Virus Templates. *Nano Lett.* **2003**, *3*, 413−417.
(8) Aldaye, F. A.; Palmer, A. L.; Sleiman, H. F. Assembling Materials with DNA as the Guide. *Science* **2008**, *321*, 1795−1799.
(9) Kim, P. Y.; Oh, J.-W.; Nam, J.-M. Controlled Co-Assembly of Nanoparticles and Polymer into Ultralong and Continuous One-Dimensional Nanochains. *J. Am. Chem. Soc.* **2015**, *137*, 8030−8033.
(10) Zhou, C.; Duan, X.; Liu, N. DNA-Nanotechnology-Enabled Chiral Plasmonics: From Static to Dynamic. *Acc. Chem. Res.* **2017**, *50*, 2906−2914.
(11) Lee, H.-E.; Ahn, H.-Y.; Mun, J.; Lee, Y. Y.; Kim, M.; Cho, N. H.; Chang, K.; Kim, W. S.; Rho, J.; Nam, K. T. Amino-Acid and Peptide-Directed Synthesis of Chiral Plasmonic Gold Nanoparticles. *Nature* **2018**, *556*, 360−365.
(12) Leibler, L. Theory of Microphase Separation in Block Copolymers. *Macromolecules* **1980**, *13*, 1602−1617.
(13) Bates, F. S.; Fredrickson, G. H. Block Copolymer Thermodynamics: Theory and Experiment. *Annu. Rev. Phys. Chem.* **1990**, *41*, 525−557.
(14) Bates, F. S.; Hillmyer, M. A.; Lodge, T. P.; Bates, C. M.; Delaney, K. T.; Fredrickson, G. H. Multiblock Polymers: Panacea or Pandora's Box? *Science* **2012**, *336*, 434−440.
(15) Balazs, A. C.; Emrick, T.; Russell, T. P. Nanoparticle Polymer Composites: Where Two Small Worlds Meet. *Science* **2006**, *314*, 1107−1110.
(16) Lee, J.-Y.; Zhang, Q.; Emrick, T.; Crosby, A. J. J. Nanoparticle Alignment and Repulsion during Failure of Glassy Polymer Nanocomposites. *Macromolecules* **2006**, *39*, 7392−7396.
(17) Thorkelsson, K.; Bai, P.; Xu, T. Self-Assembly and Applications of Anisotropic Nanomaterials: A Review. *Nano Today* **2015**, *10*, 48−66.
(18) Ouk Kim, S.; Solak, H. H.; Stoykovich, M. P.; Ferrier, N. J.; de Pablo, J. J.; Nealey, P. F. Epitaxial Self-Assembly of Block Copolymers on Lithographically Defined Nanopatterned Substrates. *Nature* **2003**, *424*, 411−414.
(19) Bita, I.; Yang, J. K. W.; Jung, Y. S.; Ross, C. A.; Thomas, E. L.; Berggren, K. K. Graphoepitaxy of Self-Assembled Block Copolymers on Two-Dimensional Periodic Patterned Templates. *Science* **2008**, *321*, 939−943.
(20) Kim, S. Y.; Nunns, A.; Gwyther, J.; Davis, R. L.; Manners, I.; Chaikin, P. M.; Register, R. A. Large-Area Nanosquare Arrays from Shear-Aligned Block Copolymer Thin Films. *Nano Lett.* **2014**, *14*, 5698−5705.
(21) Liedel, C.; Pester, C. W.; Ruppel, M.; Urban, V. S.; Böker, A. Beyond Orientation: The Impact of Electric Fields on Block Copolymers. *Macromol. Chem. Phys.* **2012**, *213*, 259−269.
(22) Majewski, P. W.; Yager, K. G. Rapid Ordering of Block Copolymer Thin Films. *J. Phys.: Condens. Matter* **2016**, *28*, 403002.
(23) Yong, D.; Jin, H. M.; Kim, S. O.; Kim, J. U. Laser-Directed Self-Assembly of Highly Aligned Lamellar and Cylindrical Block Copolymer Nanostructures: Experiment and Simulation. *Macromolecules* **2018**, *51*, 1418−1426.
(24) Hashimoto, T.; Bodycomb, J.; Funaki, Y.; Kimishima, K. The Effect of Temperature Gradient on the Microdomain Orientation of Diblock Copolymers Undergoing an Order-Disorder Transition. *Macromolecules* **1999**, *32*, 952−954.
(25) Berry, B. C.; Bosse, A. W.; Douglas, J. F.; Jones, R. L.; Karim, A. Orientational Order in Block Copolymer Films Zone Annealed below the Order-Disorder Transition Temperature. *Nano Lett.* **2007**, *7*, 2789−2794.
(26) Mita, K.; Tanaka, H.; Saijo, K.; Takenaka, M.; Hashimoto, T. Cylindrical Domains of Block Copolymers Developed via Ordering under Moving Temperature Gradient. *Macromolecules* **2007**, *40*, 5923−5933.
(27) Singh, G.; Yager, K. G.; Smilgies, D.-M.; Kulkarni, M. M.; Bucknall, D. G.; Karim, A. Tuning Molecular Relaxation for Vertical Orientation in Cylindrical Block Copolymer Films via Sharp Dynamic Zone Annealing. *Macromolecules* **2012**, *45*, 7107−7117.
(28) Samant, S.; Strzalka, J.; Yager, K. G.; Kisslinger, K.; Grolman, D.; Basutkar, M.; Salunke, N.; Singh, G.; Berry, B.; Karim, A. Ordering Pathway of Block Copolymers under Dynamic Thermal Gradients Studied by in Situ GISAXS. *Macromolecules* **2016**, *49*, 8633−8642.
(29) Zhang, R.; Singh, G.; Dang, A.; Dai, L.; Bockstaller, M. R.; Akgun, B.; Satija, S.; Karim, A. Nanoparticle-Driven Orientation Transition and Soft-Shear Alignment in Diblock Copolymer Films via Dynamic Thermal Gradient Field. *Macromol. Rapid Commun.* **2013**, *34*, 1642−1647.
(30) Samant, S.; Hailu, S. T.; Al-Enizi, A. M.; Karim, A.; Raghavan, D. Orientation Control in Nanoparticle Filled Block Copolymer Cold Zone Annealed Films. *J. Polym. Sci., Part B: Polym. Phys.* **2015**, *53*, 604−614.
(31) Yan, L.-T.; Xie, X.-M. Computational Modeling and Simulation of Nanoparticle Self-Assembly in Polymeric Systems: Structures, Properties and External Field Effects. *Prog. Polym. Sci.* **2013**, *38*, 369−405.
(32) Thompson, R. B.; Ginzburg, V. V.; Matsen, M. W.; Balazs, A. C. Predicting the Mesophases of Copolymer-Nanoparticle Composites. *Science* **2001**, *292*, 2469−2472.
(33) Kang, H.; Detcheverry, F. A.; Mangham, A. N.; Stoykovich, M. P.; Daoulas, K. C.; Hamers, R. J.; Müller, M.; de Pablo, J. J.; Nealey, P. F. Hierarchical Assembly of Nanoparticle Superstructures from Block Copolymer-Nanoparticle Composites. *Phys. Rev. Lett.* **2008**, *100*, 148303.
(34) Zhang, L.; Lin, J. Hierarchically Ordered Nanocomposites Self-Assembled from Linear-Alternating Block Copolymer/Nanoparticle Mixture. *Macromolecules* **2009**, *42*, 1410−1414.
(35) Qi, S.; Behringer, H.; Schmid, F. Using Field Theory to Construct Hybrid Particle-Continuum Simulation Schemes with Adaptive Resolution for Soft Matter Systems. *New J. Phys.* **2013**, *15*, 125009.
(36) Koski, J.; Chao, H.; Riggleman, R. A. Field Theoretic Simulations of Polymer Nanocomposites. *J. Chem. Phys.* **2013**, *139*, 244911.
(37) Raman, V.; Sharma, R.; Hatton, T. A.; Olsen, B. D. Magnetic Field Induced Morphological Transitions in Block Copolymer/Superparamagnetic Nanoparticle Composites. *ACS Macro Lett.* **2013**, *2*, 655−659.
(38) Raman, V.; Hatton, T. A.; Olsen, B. D. Kinetics of Magnetic Field-Induced Orientational Ordering in Block Copolymer/Superparamagnetic Nanoparticle Composites. *Macromol. Rapid Commun.* **2014**, *35*, 2005−2011.
(39) Diaz, J.; Pinna, M.; Zvelindovsky, A. V.; Pagonabarraga, I. Nonspherical Nanoparticles in Block Copolymer Composites: Nanosquares, Nanorods, and Diamonds. *Macromolecules* **2019**, *52*, 8285−8294.
(40) Sides, S. W.; Kim, B. J.; Kramer, E. J.; Fredrickson, G. H. Hybrid Particle-Field Simulations of Polymer Nanocomposites. *Phys. Rev. Lett.* **2006**, *96*, 250601.
(41) Zhang, Q.; Zhang, L.; Lin, J. Percolating Behavior of Nanoparticles in Block Copolymer Host: Hybrid Particle-Field Simulations. *J. Phys. Chem. C* **2017**, *121*, 23705−23715.

https://dx.doi.org/10.1021/acs.macromol.0c00101
Macromolecules 2020, 53, 2111−2122

(42) Zhang, Q.; Gu, J.; Zhang, L.; Lin, J. Diverse Chiral Assemblies of Nanoparticles Directed by Achiral Block Copolymers via Nanochannel Confinement. *Nanoscale* **2019**, *11*, 474−484.
(43) Fraaije, J. G. E. M.; van Vlimmeren, B. A. C.; Maurits, N. M.; Postma, M.; Evers, O. A.; Hoffmann, C.; Altevogt, P.; Goldbeck-Wood, G. The Dynamic Mean-Field Density Functional Method and its Application to the Mesoscopic Dynamics of Quenched Block Copolymer Melts. *J. Chem. Phys.* **1997**, *106*, 4260−4269.
(44) Zhang, L.; Sevink, A.; Schmid, F. Hybrid Lattice Boltzmann/Dynamic Self-Consistent Field Simulations of Microphase Separation and Vesicle Formation in Block Copolymer Systems. *Macromolecules* **2011**, *44*, 9434−9447.
(45) Cong, Z.; Zhang, L.; Wang, L.; Lin, J. Understanding the Ordering Mechanisms of Self-Assembled Nanostructures of Block Copolymers during Zone Annealing. *J. Chem. Phys.* **2016**, *144*, 114901.
(46) Wan, X.; Gao, T.; Zhang, L.; Lin, J. Ordering Kinetics of Lamella-Forming Block Copolymers under the Guidance of Various External Fields Studied by Dynamic Self-Consistent Field Theory. *Phys. Chem. Chem. Phys.* **2017**, *19*, 6707−6720.
(47) Zhang, L.; Liu, L.; Lin, J. Well-Ordered Self-Assembled Nanostructures of Block Copolymer Films via Synergistic Integration of Chemoepitaxy and Zone Annealing. *Phys. Chem. Chem. Phys.* **2018**, *20*, 498−508.
(48) Fredrickson, G. H. *The Equilibrium Theory of Inhomogeneous Polymers*; Oxford University Press: Oxford, 2006.
(49) Hall, D. M.; Lookman, T.; Banerjee, S. Non-Equilibrium Particle-Field Simulations of Polymer-Nanocomposite Dynamics. *Chem. Eng. Sci.* **2009**, *64*, 4754−4757.
(50) Nakayama, Y.; Kim, K.; Yamamoto, R. Simulating (Electro)-Hydrodynamic Effects in Colloidal Dispersions: Smoothed Profile Method. *Eur. Phys. J. E* **2008**, *26*, 361−368.
(51) Chiu, J. J.; Kim, B. J.; Kramer, E. J.; Pine, D. J. Control of Nanoparticle Location in Block Copolymers. *J. Am. Chem. Soc.* **2005**, *127*, 5036−5037.
(52) Mout, R.; Moyano, D. F.; Rana, S.; Rotello, V. M. Surface Functionalization of Nanoparticles for Nanomedicine. *Chem. Soc. Rev.* **2012**, *41*, 2539−2544.
(53) Phillies, G. D. J. Universal Scaling Equation for Self-Diffusion by Macromolecules in Solution. *Macromolecules* **1986**, *19*, 2367−2376.
(54) Kuksenok, O.; Travasso, R. D. M.; Balazs, A. C. Dynamics of Ternary Mixtures with Photosensitive Chemical Reactions: Creating Three-Dimensionally Ordered Blends. *Phys. Rev. E* **2006**, *74*, 011502.
(55) Cai, L.-H.; Panyukov, S.; Rubinstein, M. Mobility of Nonsticky Nanoparticles in Polymer Liquids. *Macromolecules* **2011**, *44*, 7853−7863.
(56) Carroll, B.; Bocharova, V.; Carrillo, J.-M. Y.; Kisliuk, A.; Cheng, S.; Yamamoto, U.; Schweizer, K. S.; Sumpter, B. G.; Sokolov, A. P. Diffusion of Sticky Nanoparticles in a Polymer Melt: Crossover from Suppressed to Enhanced Transport. *Macromolecules* **2018**, *51*, 2268−2275.
(57) Kim, B. J.; Chiu, J. J.; Yi, G.-R.; Pine, D. J.; Kramer, E. J. Nanoparticle-Induced Phase Transitions in Diblock-Copolymer Films. *Adv. Mater.* **2005**, *17*, 2618−2622.
(58) He, J.; Tangirala, R.; Emrick, T.; Russell, T. P.; Böker, A.; Li, X.; Wang, J. Self-Assembly of Nanoparticle−Copolymer Mixtures: A Kinetic Point of View. *Adv. Mater.* **2007**, *19*, 381−385.
(59) Ploshnik, E.; Langner, K. M.; Halevi, A.; Ben-Lulu, M.; Müller, A. H. E.; Fraaije, J. G. E. M.; Agur Sevink, G. J.; Shenhar, R. Hierarchical Structuring in Block Copolymer Nanocomposites through Two Phase-Separation Processes Operating on Different Time Scales. *Adv. Funct. Mater.* **2013**, *23*, 4215−4226.
(60) Huang, J.; Xiao, Y.; Xu, T. Achieving 3-D Nanoparticle Assembly in Nanocomposite Thin Films via Kinetic Control. *Macromolecules* **2017**, *50*, 2183−2188.
(61) Hashimoto, T. "Mechanics" of Molecular Assembly: Real-Time and In-Situ Analysis of Nano-to-Mesoscopic Scale Hierarchical Structures and Nonequilibrium Phenomena. *Bull. Chem. Soc. Jpn.* **2005**, *78*, 1−39.
(62) Travasso, R. D. M.; Kuksenok, O.; Balazs, A. C. Exploiting Photoinduced Reactions in Polymer Blends to Create Hierarchically Ordered, Defect-Free Materials. *Langmuir* **2006**, *22*, 2620−2628.
(63) Liu, Y.; Kuksenok, O.; Balazs, A. C. Coassembly of Nanorods and Photosensitive Binary Blends: "Combing" with Light To Create Periodically Ordered Nanocomposites. *Langmuir* **2013**, *29*, 750−760.
(64) Liu, Y.; Kuksenok, O.; Balazs, A. C. Using Light To Guide the Motion of Nanorods in Photoresponsive Binary Blends: Designing Hierarchically Structured Nanocomposites. *Langmuir* **2013**, *29*, 12785−12795.
(65) de Gennes, P. G. *Scaling Concepts in Polymer Physics*; Cornell University Press: Ithaca, NY, 1979.
(66) Paradiso, S. P.; Delaney, K. T.; García-Cervera, C. J.; Ceniceros, H. D.; Fredrickson, G. H. Block Copolymer Self Assembly during Rapid Solvent Evaporation: Insights into Cylinder Growth and Stability. *ACS Macro Lett.* **2014**, *3*, 16−20.
(67) Xu, X.; Man, X.; Doi, M.; Ou-Yang, Z.-c.; Andelman, D. Defect Removal by Solvent Vapor Annealing in Thin Films of Lamellar Diblock Copolymers. *Macromolecules* **2019**, *52*, 9321−9333.
(68) Delaney, K. T.; Fredrickson, G. H. Polymer Field-Theory Simulations on Graphics Processing Units. *Comput. Phys. Commun.* **2013**, *184*, 2102−2110.

https://dx.doi.org/10.1021/acs.macromol.0c00101
Macromolecules 2020, 53, 2111−2122